Translational Oncology 14 (2021) 100915

Contents lists available at ScienceDirect

Translational Oncology

journal homepage: www.elsevier.com/locate/tranon

Identification of AR-V7 downstream genes commonly targeted by AR/AR-V7 and specifically targeted by AR-V7 in castration resistant prostate cancer

Masahiro Sugiura[a,b], Hiroaki Sato[a,b], Atsushi Okabe[b], Masaki Fukuyo[b], Yasunobu Mano[b], Ken-ichi Shinohara[b], Bahityar Rahmutulla[b], Kosuke Higuchi[a,c], Maihulan Maimaiti[a], Manato Kanesaka[a,b], Yusuke Imamura[a], Tomomi Furihata[c], Shinichi Sakamoto[a], Akira Komiya[a], Naohiko Anzai[c], Yoshikatsu Kanai[d], Jun Luo[e], Tomohiko Ichikawa[a], Atsushi Kaneda[b,*]

[a] Department of Urology, Graduate School of Medicine, Chiba University, Chiba, Japan
[b] Department of Molecular Oncology, Graduate School of Medicine, Chiba University, Inohana 1-8-1, Chuo-ku, Chiba, Japan
[c] Department of Pharmacology, Graduate School of Medicine, Chiba University, Chiba, Japan
[d] Department of Bio-system Pharmacology, Graduate School of Medicine, Osaka University, Osaka, Japan
[e] Department of Urology, James Buchanan Brady Urological Institute, Johns Hopkins University, Baltimore, MD, USA

ARTICLE INFO

Keywords:
Castration-resistant prostate cancer (CRPC)
Androgen receptor (AR)
AR-V7
NUP210
SLC3A2

ABSTRACT

Primary prostate cancer (PC) progresses to castration-resistant PC (CRPC) under androgen deprivation therapy, by mechanisms e.g. expression of androgen receptor (AR) splice variant-7 (AR-V7). Here we conducted comprehensive epigenome and transcriptome analyses comparing LNCaP, primary PC cells, and LNCaP95, AR-V7-expressing CRPC cells derived from LNCaP. Of 399 AR-V7 target regions identified through ChIP-seq analysis, 377 could be commonly targeted by hormone-stimulated AR, and 22 were specifically targeted by AR-V7. Among genes neighboring to these AR-V7 target regions, 78 genes were highly expressed in LNCaP95, while AR-V7 knockdown led to significant repression of these genes and suppression of growth of LNCaP95. Of the 78 AR-V7 target genes, 74 were common AR/AR-V7 target genes and 4 were specific AR-V7 target genes; their most suppressed genes by AR-V7 knockdown were *NUP210* and *SLC3A2*, respectively, and underwent subsequent analyses. *NUP210* and *SLC3A2* were significantly upregulated in clinical CRPC tissues, and their knockdown resulted in significant suppression of cellular growth of LNCaP95 through apoptosis and growth arrest. Collectively, AR-V7 contributes to CRPC proliferation by activating both common AR/AR-V7 target and specific AR-V7 target, e.g. *NUP210* and *SLC3A2*.

1. Introduction

Prostate cancer (PC) is a major cause of cancer death among men, where androgen receptor (AR) plays important role in its progression [1]. Although androgen deprivation therapy (ADT) is considered as standard treatment against primary PC and is initially effective, PC acquires resistance to ADT and progresses to lethal castration-resistant prostate cancer (CRPC) [2, 3]. Despite castration levels of testosterone, most CRPC cases continue to rely on AR signalling [4]. While next generation hormonal therapies, such as abiraterone and enzalutamide, have been approved for CRPC treatment, most patients eventually acquire resistance to these drugs [3, 5].

The mechanisms of CRPC development reportedly include amplification or overexpression of AR, expression of AR splice variants (AR-Vs), mutation of AR, mutations in coactivators/corepressors, androgen-independent AR activation, and intratumoral androgen production [6–9]. Among these, AR-Vs reportedly play important role in CRPC [10]. Among >20 different AR-Vs that have been identified in clinical PC and PC cell lines [3], AR splice variant 7 (AR-V7) is associated with resistance to next generation ADTs and poor cancer-specific survival [11].

Abbreviations: PC, prostate cancer; CRPC, castration-resistant PC; AR, androgen receptor; AR-V, AR splice variant; AR-V7, AR splice variant-7; ADT, androgen deprivation therapy; LBD, ligand-binding domain; DHT, dihydrotestosterone; GO, gene ontology; GSEA, gene set enrichment analysis; qPCR, quantitative PCR; RNA-seq, RNA sequencing; ChIP, Chromatin Immunoprecipitation; ChIP-seq, ChIP sequencing; shRNA, small hairpin RNA; SA-β-Gal, senescence-associated β-galactosidase; FAIRE, formaldehyde-assisted isolation of regulatory elements.

* Corresponding author.
E-mail address: kaneda@chiba-u.jp (A. Kaneda).

https://doi.org/10.1016/j.tranon.2020.100915
Received 20 August 2020; Received in revised form 28 September 2020; Accepted 12 October 2020

AR-V7 lacks the C-terminal ligand-binding domain (LBD), but harbors N-terminal transactivation domain and DNA binding domain. Owing to lack of LBD, AR-V7 can circumvent the pharmacological effects of next generation ADTs, such as enzalutamide, which targets LBD of AR directly, and abiraterone, an inhibitor of androgen biosynthesis.

AR-V7 is constitutively active and capable of activating canonical AR target genes even in the absence of androgen [12, 13]. Although identification and characterization of AR-V7 target genes have been conducted by several studies [14], not a single gene targeted by AR-V7 was found to be upregulated in ≥2 of these studies, and the regulatory function of AR-V7 different from AR is still mostly unknown. Furthermore, it is still controversial whether AR-V7 is a principal driver or a mere marker of CRPC [14].

Comprehensive genomic analyses have revealed various genomic abnormalities including AR in primary PC and CRPC over the past years. In addition to genomic abnormalities, epigenomic alterations, such as aberrant histone modifications, reportedly associate with cancer progression including PC. H3K4me1, H3K4me3 and H3K27ac are major histone epigenetic modification marks. H3K4me1 commonly associates with active enhancers, H3K4me3 is highly enriched at active promotors, and H3K27ac is known as an active transcription mark [15].

To elucidate the role of AR-V7 in CRPC, we here perform a comprehensive analysis of transcriptome and epigenome through evaluation of RNA-seq and ChIP-seq data for H3H4me1, H3K4me3, H3K27ac, AR and AR-V7 comparing LNCaP, primary PC cells, and LNCaP95, AR-V7-expressing CRPC cells derived from LNCaP. We report landscape of AR-V7 target regions, and 78 AR-V7 downstream target genes including 74 genes commonly targeted by AR and AR-V7 and 4 genes targeted specifically by AR-V7. Our data shows that AR-V7 contributes to CRPC proliferation through activation of both common AR/AR-V7 target gene and specific AR-V7 target gene.

2. Materials and methods

Detailed information is fully described in the Supporting Methods.

2.1. Cell culture

The human PC cell line LNCaP was obtained from American Type Culture Collection (Manassas, VA). LNCaP was cultured in RPMI-1640 supplemented with 10% FBS. LNCaP95 is previously established CRPC cell line expressing AR-V7 derived from LNCaP [16]. LNCaP95 was cultured in phenol red-free RPMI-1640 supplemented with 10% charcoal-stripped serum.

2.2. Western blot analysis

Western blotting was performed as previously described [17], using antibodies against AR (#06-680, Millipore, Billerica, MA), AR-V7 (#31-1109-00, RevMAb Biosciences, South San Francisco, CA), SLC3A2 (#15193-1-AP, Proteintech Group, Rosemont, IL), SLC7A5 (#sc-374232, Santa Cruz Biotechnology), and NUP210 (#A301-795A, Bethyl Laboratories, Montgomery, TX). Antibodies against Actin (#ab14128, Abcam, Cambridge, MA), Lamin A and Aldolase (#sc-20680 and #sc-12059, Santa Cruz Biotechnology, Santa Cruz, CA) were used as loading control for whole cell lysates, nuclear proteins, and cytoplasmic protein, respectively. Original full images of western blot analysis were shown in Fig. S1.

2.3. Quantitative RT-PCR (RT-qPCR)

Quantification by PCR was performed as previously described [18]. The PCR primers were listed in Table S1.

2.4. RNA extraction, library construction, and RNA sequencing (RNA-seq) analysis

Total RNA was isolated using RNeasy Mini Kit (Qiagen, Hilden, Germany) according to manufacturer's protocol, and treated with DNaseI (Qiagen). RNA-seq analysis was performed as previously described [19]. TruSeq Stranded mRNA Sample Prep Kit (Illumina, San Diego, CA) was used to prepare the library for RNA-seq. Deep sequencing was performed on Illumina HiSeq 1500 or NextSeq 500 platform using TruSeq Rapid SBS Kit (Illumina).

2.5. Chromatin Immunoprecipitation (ChIP) assay

ChIP assay were performed as reported [18]. Antibodies against AR (#06-680, Millipore), H3K4me3 (#ab8580, Abcam), H3K27ac (#39135, Active Motif, Carlsbad, CA), and H3K4me1 (#ab8895, Abcam), and Protein G-sepharose beads (GE Healthcare, Tokyo, Japan) or Dynabeads (Life technologies, Carlsbad, CA), were used. Primer sequences for ChIP-qPCR were listed in Table S2.

2.6. ChIP sequencing (ChIP-seq) analysis

ChIP-seq analysis was performed as described [20]. ChIP libraries were constructed using NEBNext ChIP-seq Library Prep Reagent Set for Illumina (NEB, Ipswich, MA), quantified using Bioanalyzer (Agilent, Santa Clara, CA), and sequenced at concentration of 4 pM on Illumina Hiseq (Illumina).

2.7. Knockdown by small hairpin RNA (shRNA)

We performed knockdown experiment using shRNA as described [19]. Oligonucleotide sequences for shRNAs against AR-V7 (shAR-V7#1 and #2) and control non-target shRNA (shNon) were described in Table S3.

2.8. Knockdown by siRNA

siRNAs targeting *SLC3A2* (siSLC3A2#1: HSS109825 and #2: HSS109826), *NUP210* (siNUP210#1: HSS118399, and #2: HSS177269), and *SLC7A5* (siSLC7A5#1: HSS112004 and #2: HSS188571), and the control siRNA (siCTRL: 12935113) were purchased from Invitrogen (Carlsbad, CA). Cells were transfected with siRNA using OPTI-MEN (Invitrogen) and Lipofectamine RNAiMax Reagent (Invitrogen) according to manufacturer's protocol.

2.9. Cell proliferation assay

Following treatment with shRNA or siRNA, cells were seeded in 96-well plates. Cell proliferation was determined using Cell Counting kit8 (CCK8) (Dojindo, Kumamoto, Japan).

2.10. Flow cytometric analysis

Cell cycle analysis was performed using cell sorter HS800 (Sony, Tokyo, Japan) as described [21]. Flow cytometry data were analyzed using FlowJo (https://www.flowjo.com/).

2.11. Annexin V-FITC apoptosis assay

Cells were transfected with siRNA for 120 h, and were analyzed using Annexin V-FITC Apoptosis Detection Kit (Abcam) according to manufacturer's protocol.

2.12. Caspase-3/7 apoptosis staining

Analysis of apoptosis staining was performed using CellEvent Caspase-3/7 Green Detection Reagent (Caspase-3/7) (Invitrogen).

2.13. Senescence-associated β-galactosidase (SA-β-Gal) staining

Cellular senescence was analyzed via SA-β-Gal staining as previously described [18, 22]. As reported [18], we used the mouse embryonic fibroblasts (MEF) infected with retrovirus of oncogenic *Ras* and those with mock retrovirus as control samples of SA-β-Gal(+) and SA-β-Gal(-) cells, respectively (Fig. S2.).

2.14. Formaldehyde-assisted isolation of regulatory elements (FAIRE)

FAIRE was performed as previously reported [23]. Primer sequences for FAIRE-qPCR were listed in Table S4.

2.15. Analysis of clinical PC datasets

Grasso was obtained through GEO datasets (https://www.ncbi.nlm.nih.gov/geo/) (GSE35988) [24], and the Cancer Genome Atlas (TCGA) (http://www.cancergenome.nih.gov/) was obtained through Oncomine (https://www.oncomine.org/resource/login.html).

2.16. Statistical analysis

Gene expression levels were compared using t-test. Kolmogorov-Smirnov test was performed to evaluate the distribution of AR-V7 target genes. $P<0.05$ was considered as statistically significant. Gene ontology (GO) analysis was performed using Metascape (http://metascape.org/gp/index.html#/main/step1), where $P<1\times10^{-4}$ was considered statistically significant. Gene set enrichment analysis (GSEA) was performed using GSEA v3.0 software (https://software.broadinstitute.org/gsea/index.jsp).

2.17. Data access

Genome-wide analysis data were submitted to GEO datasets. Accession numbers for RNA-seq and ChIP-seq data were GSE122923 (GSM3488649- GSM3488684) and GSE122922 (GSM3488490-GSM3488508), respectively.

3. Results

3.1. Expression of AR-V7 and its contribution in CRPC cellular growth

To determine protein expression and localization of AR and AR-V7 in PC cells, we treated LNCaP with dihydrotestosterone (DHT), and performed western blot analysis. DHT treatment caused a significant increase in nuclear AR expression, but AR-V7 expression was not detected regardless of the presence or absence of DHT (Fig. 1A, Fig. S1A).

Gene expression alteration following DHT treatment was analysed by RNA-seq. When 674 genes upregulated by >1.5-fold following DHT stimulation in LNCaP were extracted, gene upregulation was most apparently observed at 6 or 12 h after DHT stimulation, and the most upregulated genes included AR target gene *KLK2* (Fig. 1B). ChIP-seq for H3K4me3, H3K4me1, H3K27ac and AR was conducted to analyse epigenomic alteration between before and 12 h after DHT stimulation. H3K4me3(+) regions were defined as promoters, whereas H3K4me1(+) regions without H3K4me3 peaks were defined as enhancers. Epigenetic status around *TMPRSS2* representatively showed AR binding to enhancer regions with increase of H3K27ac following DHT treatment (Fig. S3). Enhancers were more preferentially targeted by AR than promoters, and these enhancer regions showed significant enrichment of AR and FOXA1 motifs (Fig. S4), which is consistent with the previous report that FOXA1 is a pioneer factor for AR in PC [25, 26].

Western blot analysis was also conducted using LNCaP95 (Fig. 1C, Fig. S1B). While DHT caused a significant increase in nuclear AR expression in LNCaP95 similar to LNCaP, AR-V7 expression in the nucleus was confirmed regardless of DHT stimulation. In RNA-seq (Fig. 1D), genes upregulated by DHT stimulation in LNCaP were significantly upregulated in LNCaP95 in the absence of DHT, and gene expression levels in LNCaP95 were not markedly altered by DHT stimulation compared to LNCaP, which is consistent to nuclear expression of AR-V7 in LNCaP95.

In ChIP-seq against LNCaP95, antibodies against AR/AR-Vs recognizes N-terminal region of AR and AR-Vs commonly. AR/AR-Vs binding regions were mostly enhancers and these enhancer regions also showed significant enrichment of AR and FOXA1 motifs (Fig. S5). Enhancer region of *SLC25A33* representatively showed binding of AR/AR-Vs in the absence of DHT stimulation, with high H3K27ac signal in both absence and presence of DHT stimulation (Fig. S3).

To confirm the significance of AR-V7 in CRPC cell proliferation, LNCaP95 were treated with shRNA's against AR-V7, but not against AR. Specific reduction of AR-V7 in mRNA and protein levels was confirmed by RT-qPCR and western blot analysis, respectively. Knockdown of AR-V7 markedly decreased cellular growth of LNCaP95 ($P<0.05$) (Fig. 1E-G, Fig. S1C),

3.2. Identification of AR-V7 target genes

Considering AR-V7 expression and binding in LNCaP95 in the absence of DHT, and no AR-V7 expression in LNCaP (Fig. 1), we extracted candidate AR-V7 targets by comparing AR/AR-Vs peaks between LNCaP and LNCaP95 (Fig. 2A). Among 550 AR/AR-Vs binding regions in LNCaP95 in the absence of DHT, 151 regions also showed peaks in LNCaP in the absence of DHT, which were considered as noise of genome-wide analysis or AR binding regions even in the absence of DHT. The residual 399 regions were considered as candidate AR-V7 target regions (Fig. 2B). Of 399 regions, 377 overlapped with 33,247 AR peaks in LNCaP after DHT stimulation (Fig. 2C), indicating that AR-V7 mostly binds and activates AR-target regions in hormone-depleted condition. The residual 22 peaks were considered as AR-V7 specific target regions, which were not bound by DHT-stimulated AR in LNCaP (Fig. 2C).

The 399 AR-V7 target regions were annotated to neighboring genes, using Genomic Regions Enrichment of Annotations Tool (GREAT) [27], and 496 neighboring genes were identified. Since AR-V7 is expressed specifically in LNCaP95, 78 genes showing >2.0-fold upregulation in LNCaP95 compared to LNCaP were extracted as AR-V7 target genes (Fig. 2D, and Table S5). These included 4 AR-V7 specific target genes, and 74 AR/AR-V7 common target genes. AR-V7 specific genes are defined as genes that show AR/AR-Vs peaks in LNCaP95 but not in LNCaP, and show higher expression level in LNCaP95 by >2.0-fold compared to LNCaP. GO analysis in 78 AR-V7 target genes is shown in Table S6. Furthermore, we investigated expression of the 78 AR-V7 target genes in PC patients using TCGA dataset by GSEA. Among the 550 enrolled patients, the top 100 patients showing high expression of AR-V7 and the bottom 100 patients showing low expression of AR-V7 are defined as AR-V7 high and low groups, respectively. The 78 target genes were shown to be significantly upregulated in AR-V7 high group (Fig. S6A) (NES=1.24, FDR=0.14). Significant enrichment of Hallmark pathways was also investigated using 50 MSigDB HALLMARK gene sets; epithelial mesenchymal transition (EMT) pathway showed the most significant upregulation in AR-V7 high group (Fig. S6B).

Furthermore, gene expression alteration in LNCaP95 following shAR-V7 treatment was analyzed by RNA-seq (Fig. 2E). When genes were sorted in the order from upregulated to downregulated level after AR-V7 knockdown, significant enrichment to the downregulated genes was observed in AR-V7 specific target genes ($P=0.04$) and AR/AR-V7 common target genes ($P=0.02$) (Fig. 2E). The total of 78 AR-V7 target genes were negatively correlated with genes upregulated by shAR-V7 (NES=-2.04, FDR<0.001). Among 78 genes, *NUP210* and *SLC3A2* that were the most downregulated AR/AR-V7 common target gene and the most downregulated AR-V7 specific target gene, respectively, underwent subsequent analyses.

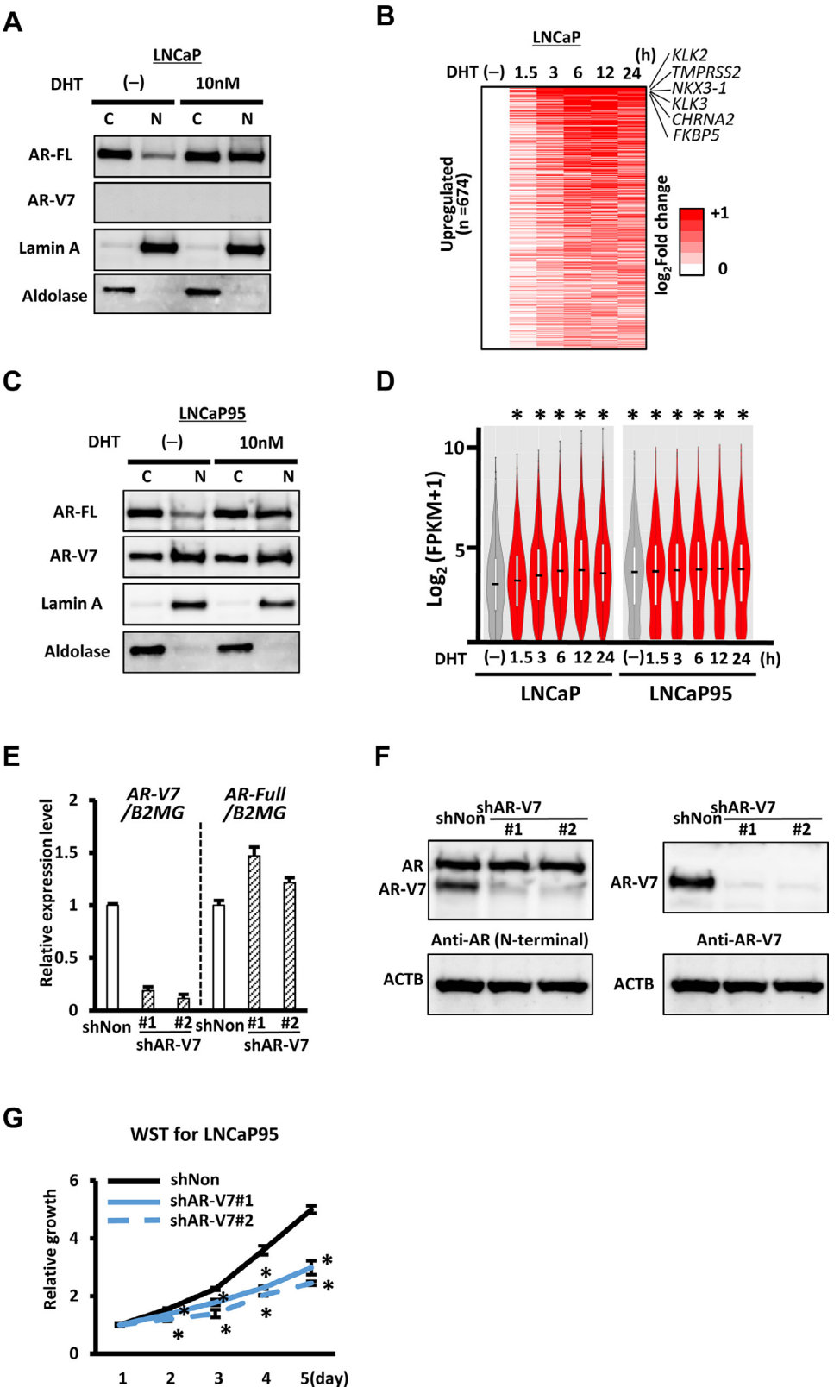

Fig. 1. AR and AR-V7 expression in LNCaP and LNCaP95. (A) Western blot analysis of AR and AR-V7 in LNCaP. *AR-FL*, AR full length. *C*, cystoplasmic extract. *N*, nuclear extract. Lamin A and Aldolase were nuclear and cytoplasmic markers, respectively. In presence of 10 nM DHT, AR was increased in nuclear fraction, and no expression of AR-V7 was confirmed. **(B)** Heatmap of 674 genes upregulated by >1.5-fold after 10 nM DHT stimulation at 1.5, 3, 6, 12, or 24 h in LNCaP. Gene upregulation was most apparently observed at 6 or 12 h (*See* also Fig. 1D). **(C)** Western blot analysis of AR and AR-V7 in LNCaP95 cells in the absence or presence of DHT. AR-V7 expression in the absence of DHT and increase of AR expression in nuclear fraction in the presence of DHT were observed. (**D**) Gene expression levels in LNCaP and LNCaP95 cells after DHT stimulation. The 674 genes upregulated by >1.5-fold by DHT stimulation in LNCaP were shown to be expressed at significantly higher level in LNCaP95 even before DHT stimulation. $^{*}P<10^{-4}$, $Q<0.1$. **(E)** RT-qPCR analysis of AR and AR-V7 in LNCaP95 following shAR-V7 treatment. *#1* and *#2*, shAR-V7#1 and #2, respectively. AR-V7 was specifically knocked down by shRNA. **(F)** Western blot analysis of AR and AR-V7 in LNCaP95 cells following shAR-V7 treatment. Antibodies against common N-terminal domain of AR/AR-V7 (*left*, #06-680) and C-terminal domain specific to AR-V7 (*right*, #31-1109-00) were used. AR-V7 was specifically knocked down, while full-length AR was intact. **(G)** Suppression of cellular growth. WST-8 assay was performed to evaluate cell proliferation of LNCaP95 cells after shAR-V7 knockdown. $^{*}P<0.05$ (*t*-test). Data represent the mean ± SEM of 3 experiments.

3.3. Upregulation of NUP210 in clinical CRPC tissues

Genome browser view shows binding of AR at *NUP210* locus in DHT-treated LNCaP, and binding of AR-V7 in hormone-depleted LNCaP95 (Fig. 3A). Knockdown of AR-V7 resulted in decrease of H3K27ac levels at *NUP210* locus (Fig. 3A), and decrease of *NUP210* expression (Fig. 3B), indicating the contribution of AR-V7 to the activation of *NUP210* expression. The AR/AR-V7 target region at *NUP210* locus was analyzed by FAIRE-PCR, to confirm open chromatin status in DHT-treated LNCaP and hormone-depleted LNCaP95, and not in hormone-depleted LNCaP.

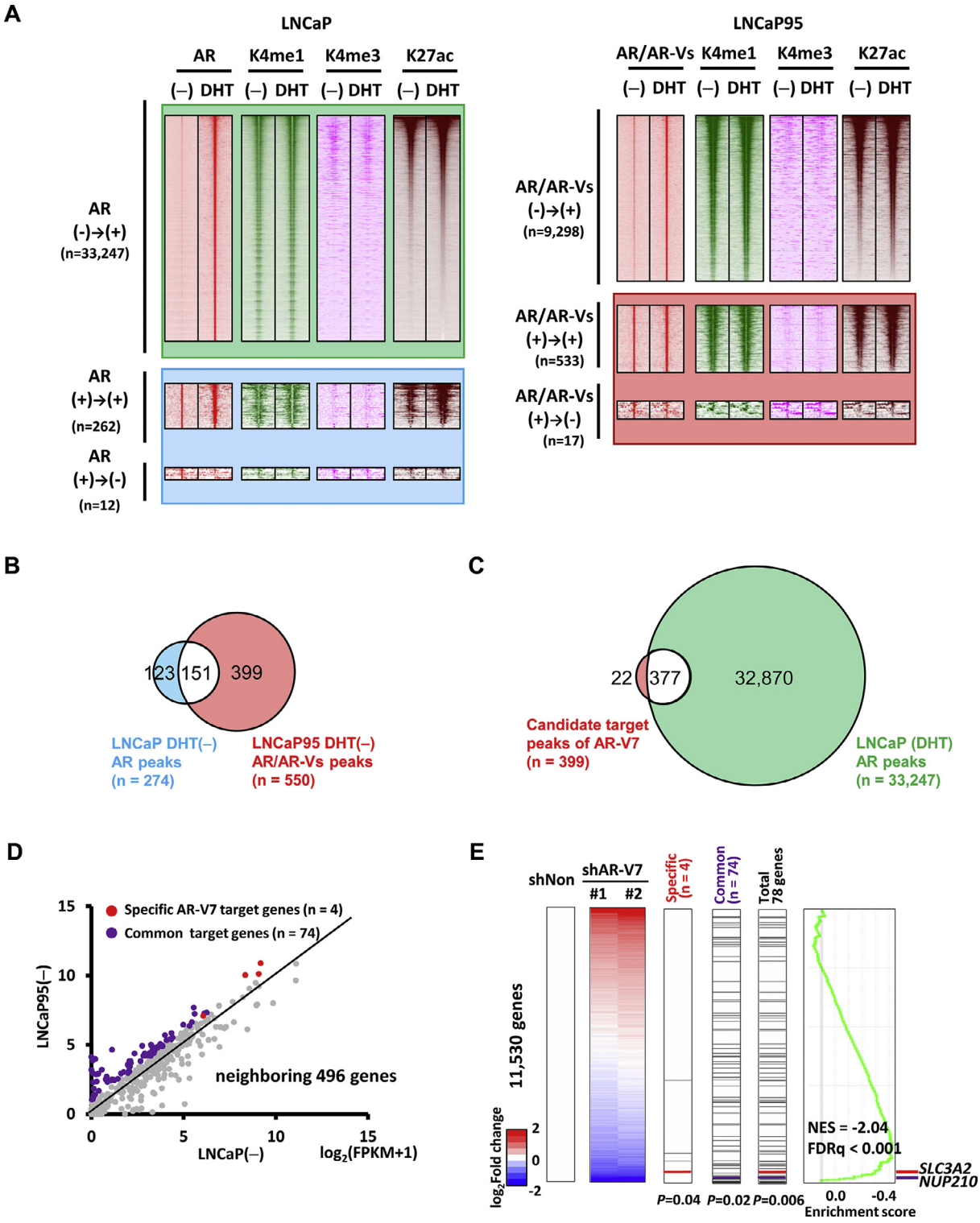

Fig. 2. Identification of AR-V7 target genes. (A) Integrated analyses of AR and histone modifications in LNCaP cells (*left*) and LNCaP95 (*right*) (*See* also Fig. S4, S5). Heatmaps represent read density of AR, H3K4me1, H3K4me3, and H3K27ac within ±5kb around AR/AR-Vs peaks. *(-)*, hormone depleted. *DHT*, stimulated by 10 nM DHT. **(B)** Extraction of candidate AR-V7 target regions. Among AR/AR-Vs peaks in hormone-depleted LNCaP95 cells (n=550), 151 peaks overlapped with AR peaks in hormone-depleted LNCaP were excluded, and the remaining 399 regions were regarded as candidate targets of AR-V7. **(C)** Overlap of candidate AR-V7 peaks (n=399) and AR peaks (n=33,247) in hormone-stimulated LNCaP. While 377 candidate AR-V7 peaks are commonly targeted by AR in hormone stimulated condition, 22 peaks were unique regions targeted specifically by AR-V7. **(D)** Identification of genes upregulated in LNCaP95. Expression levels of neighboring genes around the 399 candidate AR-V7 target regions (n=496) were compared between hormone-depleted LNCaP and LNCaP95 cells. 78 genes were upregulated by >2.0-fold in LNCaP95, including 4 specific AR-V7 target genes (*red*) and 74 common AR/AR-V7 target genes (*purple*). **(E)** Comparison of AR-V7 target genes with downregulated genes in LNCaP95 with knockdown of AR-V7. Genes altered in LNCaP95 treated with shAR-V7 were sorted by expression ratio to shNon-treated cells. The specific AR-V7 target genes (n=4, e.g. *SLC3A2, red*), the common AR/AR-V7 target genes (n=74, e.g. *NUP210, purple*), and the total of 78 genes, were all significantly enriched to the downward (*P*=0.04, *P*=0.02, *P*=0.006, respectively; Kolmogorov-Smirnov test). GSEA also showed significant enrichment of the 78 target genes to the downward.

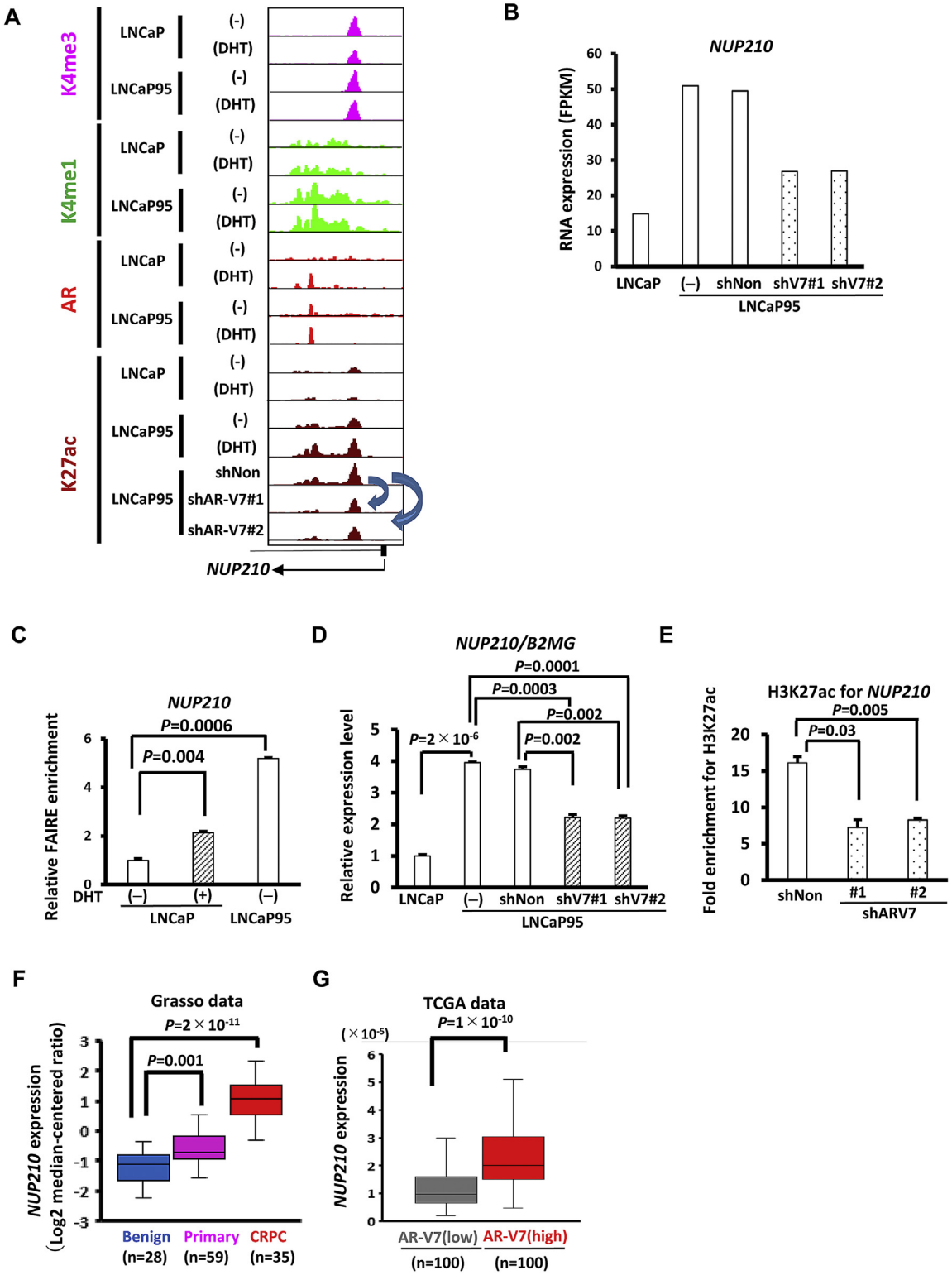

Fig. 3. *NUP210* expression in clinical datasets. (A) Epigenetic status around *NUP210*. AR binding to *NUP210* in DHT stimulated LNCaP and AR/AR-V7 binding in LNCaP95 in the absence and presence of DHT were shown. **(B)** RNA expression of *NUP210*. AR-V7 knockdown decreased FPKM value of *NUP210*. **(C)** FAIRE-qPCR analysis at AR/AR-V7 target region around *NUP210* in hormone-depleted or -stimulated LNCaP and hormone-depleted LNCaP95. **(D)** RT-qPCR analysis of *NUP210* in LNCaP and LNCaP95 cells with/without shRNA treatment. **(E)** Reduction of H3K27ac level at the *NUP210* enhancer. H3K27ac enrichment was measured by ChIP-qPCR at the AR/AR-V7 target region around *NUP210*, showing a decrease following AR-V7 knockdown. Data represent the mean ± SEM of 3 experiments. **(F)** *NUP210* expression levels in benign lesions, primary PC, and CRPC (Grasso prostate dataset). Expression of *NUP210* was elevated in primary PC compared with benign lesions (P=0.001), but markedly upregulated in CRPC ($P=2\times10^{-11}$). **(G)** *NUP210* expression levels in PC cases with higher and lower expression of *AR-V7* (TCGA PRAD dataset). Among the 550 patients enrolled in TCGA, the top 100 patients showing high expression of *AR-V7* and the bottom 100 patients showing low expression of *AR-V7* are defined as AR-V7 high and low groups, respectively.

It was validated by RT-qPCR that *NUP210* expression was low in LNCaP, high in LNCaP95, and decreased by AR-V7 knockdown ($P<0.01$). ChIP-PCR showed that H3K27ac level was decreased atAR/AR-V7 target region after AR-V7 knockdown ($P<0.05$) (Fig. 3C-3E). The Grasso dataset showed that *NUP210* was elevated in primary PC compared with benign lesion ($P=0.001$), but more markedly upregulated in clinical CRPC tissues ($P=2\times10^{-11}$). The TCGA dataset showed that *NUP210* expression was significantly higher in clinical PC patients with high AR-V7 expression compared with those with low AR-V7 expression ($P=1\times10^{-10}$) (Fig. 3F-3G).

3.4. Contribution of NUP210 to cellular growth

When LNCaP in presence of androgen and LNCaP95 in absence of androgen were treated with two siRNA's against *NUP210*, NUP210 expression was significantly repressed at mRNA and protein levels, and cellular growth was significantly suppressed ($P<0.05$) (Fig. 4A-4B, Fig. S1D). We performed apoptosis assay using Annexin-V FITC/PI staining, and cell apoptosis rate was significantly increased following *NUP210* knockdown in LNCaP95 ($P=0.001$) (Fig. 4C). In caspase-3/7 fluorescent staining, LNCaP95 displayed increased staining following *NUP210* knockdown (Fig. 4D, Fig. S7A). In cell cycle analysis, there was a significant decrease in S phase and a significant increase in G1 phase following *NUP210* knockdown, suggesting cell cycle arrest (Fig. 4E, Fig. S7B). In SA-β-Gal staining, the increase of SA-β-Gal(+) cells following *NUP210* knockdown was not statistically significant compared to siCTRL treatment ($P=0.1$) (Fig. 4F, Fig. S7C).

3.5. Upregulation of SLC3A2 in clinical CRPC tissues

At *SLC3A2* locus, binding of AR was not detected in DHT-treated LNCaP, but binding of AR-V7 was detected in hormone-depleted LNCaP95 (Fig. 5A). Knockdown of AR-V7 resulted in decrease of H3K27ac levels at *SLC3A2* locus (Fig. 5A), and decrease of *SLC3A2* expression (Fig. 5B), indicating the contribution of AR-V7 to the activation of *SLC3A2* expression. The AR/AR-V7 target region at *SLC3A2* locus was analysed by FAIRE-PCR, to confirm open chromatin status in hormone-depleted LNCaP95, and not in DHT-treated LNCaP, compared with hormone-depleted LNCaP (Fig. 5C). It was validated by RT-qPCR that *SLC3A2* expression was low in LNCaP, high in LNCaP95, and decreased by AR-V7 knockdown ($P<0.01$) (Fig. 5D). ChIP-PCR showed that H3K27ac level was decreased at the AR/AR-V7 target region after AR-V7 knockdown ($P<0.01$) (Fig. 5E) In clinical samples, *SLC3A2* expression was lower in benign lesions and primary PC tissues, and significantly higher in CRPC tissues (Fig. 5F). In another cohort, PC patients with high AR-V7 expression showed higher *SLC3A2* expression than those with low AR-V7 expression ($P=4\times10^{-4}$) (Fig. 5G).

3.6. Contribution of SLC3A2 to cellular growth

When LNCaP and LNCaP95 were treated with siRNA against *SLC3A2*, expression of SLC3A2 was significantly repressed at mRNA and protein levels, and cellular growth was significantly suppressed ($P<0.05$) (Fig. 6A-6B, Fig. S1E). Annexin-V FITC/PI staining showed significant increase of cell apoptosis rate ($P=0.01$) (Fig. 6C). Similar results were obtained in caspase-3/7 Fluorescent staining (Fig. 6D, Fig. S7D). In cell cycle analysis, there was a significant decrease in S phase and a significant increase in G1 phase following *SLC3A2* knockdown, suggesting cell cycle arrest (Fig. 6E, Fig. S7E). In SA-β-Gal staining, the number of SA-β-Gal(+) cells were markedly increased following *SLC3A2* knockdown ($P=0.003$), indicating that SLC3A2 knockdown suppressed cell proliferation through apoptosis and cellular senescence (Fig. 6F, Fig. S7F).

3.7. Involvement of E2F, G2M and EMT pathways

Gene expression alteration after knockdown of SLC3A2 in LNCaP95 was analyzed by RNA-seq. The 2,317 genes downregulated by both siSLC3A2#1 and siSLC3A2#2 were significantly associated with GO terms such as cell cycle, cell division and DNA replication (Fig. 7A). To identify enrichment of Hallmark pathways in genes whose expressions were altered by siSLC3A2, GSEA was performed against 50 MSigDB HALLMARK gene sets. In control LNCaP95 cells compared with *SLC3A2*-knockdown cells, 11 gene sets, including E2F, G2M, and EMT pathways, were significantly upregulated (NES>1.8, FDRq<0.25) (Fig. 7B). Conversely, 3 gene sets were significantly downregulated in LNCaP95 (NES<-1.6, FDRq<0.25), which were similarly downregulated in AR-V7 high group of PC patients (Fig. S6B).

4. Discussion

Nuclear AR-V7 was expressed in LNCaP95 in the absence of DHT, confirming that AR-V7 could be transcribed independently of AR under hormone-depleted conditions, and that AR-V7 could translocate into nucleus without hormone stimulation. Knockdown of AR-V7 suppressed cellular growth of LNCaP95, indicating that AR-V7 is not only expressed as a bio-marker, but functions as a principal driver for CRPC.

Several studies have examined AR-V7 downstream genes. Microarray and ChIP-PCR analysis using 22Rv1 CRPC cells demonstrated that AKT1 is unique AR-V7 target gene [28]. Lu *et al.* demonstrated the regulatory landscape of AR-Vs using 22Rv1 [29]. While these studies suggested a tumorigenic role of AR-V7, the entire landscape of AR-V7 target regions and the difference from AR targets has not been fully clarified. In this study, parental LNCaP and its castration-resistant derivative cell expressing AR-V7, LNCaP95, were compared on genome-wide scale through ChIP-seq and RNA-seq analyses. As many as 399 regions were shown to be targeted by AR-V7 in LNCaP95 in the absence of DHT. Most of AR-V7 targets (377/399 regions) were also bound by hormone-stimulated AR, indicating that AR-V7 could activate a portion of AR target regions under hormone-depleted conditions. However, a fraction of AR-V7 targets (22/399 regions) were found to be AR-V7 specific target regions, which could not be bound by hormone-stimulated AR.

Among specific AR-V7 target genes, *SLC3A2* was identified as significant AR-V7 downstream gene. SLC3A2 reportedly contributes to integrin-dependent cell spreading and protection from apoptosis [30], promoting tumor growth in various cancers including osteosarcoma, renal cancer, and breast cancer [31-33]. In our analysis, knockdown of *SLC3A2* resulted in apoptosis and cell cycle arrest in LNCaP95. SLC3A2 knockdown caused the decrease of cell proliferation in LNCaP95 as well as LNCaP, suggesting that SLC3A2 may play an important role in cell proliferation in primary PC, and that upregulation by AR-V7 may accelerate the proliferation in CRPC.

SLC3A2 in known to form a heterodimeric amino acid transporter with SLC7 family [34]. Among SLC7 family proteins, SLC7A5 is reportedly overexpressed in various cancers [35]. In PC, SLC7A5 upregulation is reportedly associated with the acquirement of CRPC and may be a druggable target for CRPC [36]. SLC3A2 interacts with SLC7A5 to control intracellular trafficking and membrane topology [37], and the SLC3A2/SLC7A5 complex associates with aggressive human cancers [38]. The expression of SLC3A2 and SLC7A5 is reportedly co-dependent, and downregulation of either subunit destabilizes the partner [39]. Genes downregulated by siSLC3A2 were associated with GO terms such as cell cycle, cell division and DNA replication. These suggests that SLC3A2 play important roles in CRPC proliferation, and could be a druggable target as well as SLC7A5.

We also investigated AR/AR-V7 common target gene, *NUP210*. Knockdown of NUP210 caused the decrease of cell proliferation in LNCaP95 as well as LNCaP, suggesting that *NUP210* targeted by AR in primary PC and by AR-V7 in CRPC may both contribute to cancer cell proliferation. Nuclear pore complexes are multiprotein transport channels which connect the nucleus and cytoplasm, and are composed of various nucleoporins [40]. Nucleoporins include POM121, which promotes CRPC through regulation of E2F1, MYC, and AR nuclear transport [41]. NUP210 reportedly shows various functions including gene

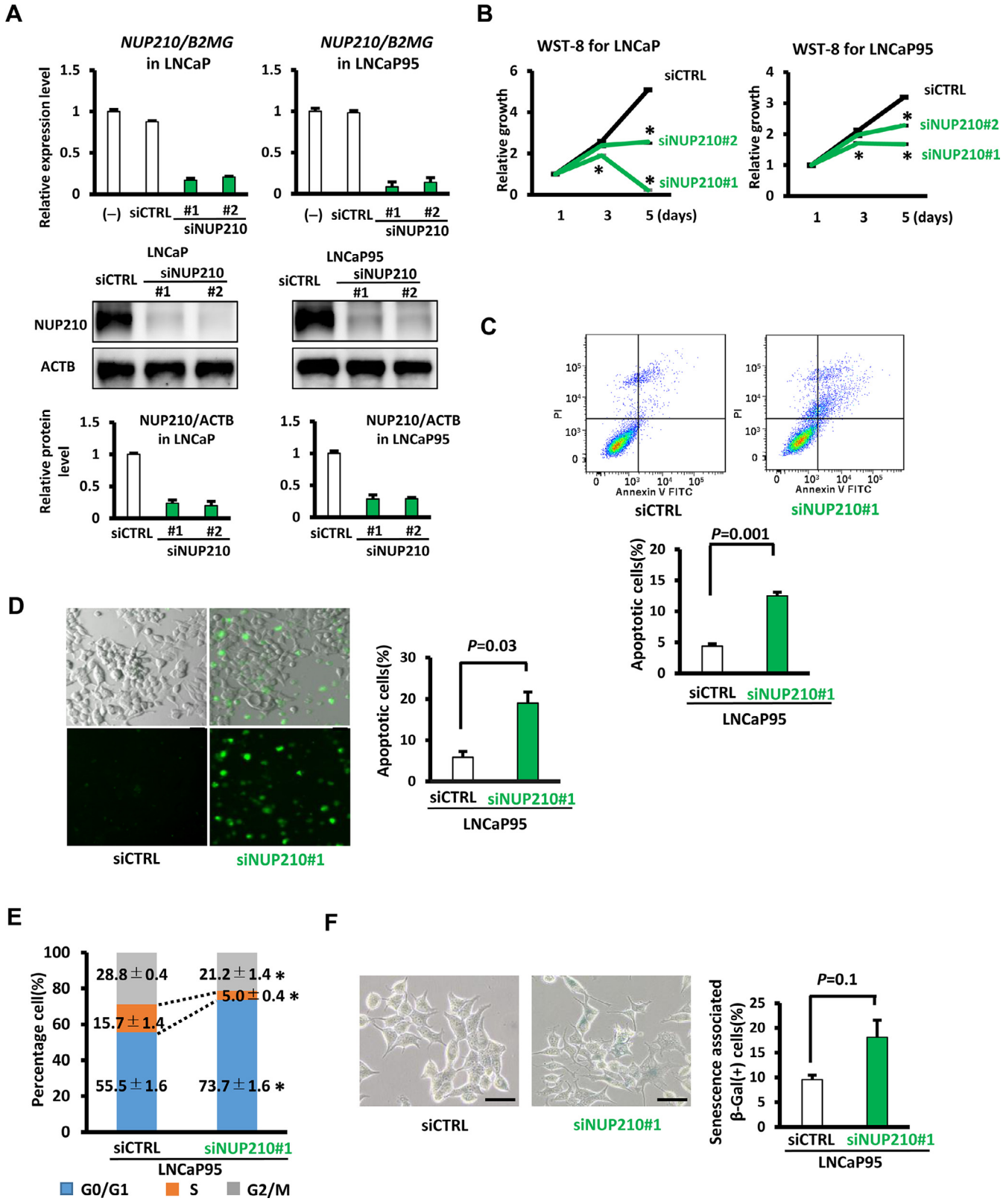

Fig. 4. Growth suppression by NUP210 knockdown. LNCaP in presence of androgen and LNCaP95 in absence of androgen were treated with siRNA's against *NUP210*. **(A)** RT-qPCR analysis of *NUP210* gene expression levels (*upper*) and western blot analysis of NUP210 protein expression levels (*lower*) in LNCaP and LNCaP95 cells following transfection with two siNUP210 (*#1* and *#2*). **(B)** WST assay for cells following NUP210 knockdown. Significant suppression of cellular growth following NUP210 knockdown was detected, in both LNCaP in hormone-stimulated condition and LNCaP95 in hormone-depleted condition. $^{*}P<0.05$ (*t*-test). **(C)** Cell apoptosis analysis by Annexin-V FITC/PI staining and flow cytometry. The cell apoptosis rate of LNCaP95 was significantly increased following NUP210 knockdown **(D)** Caspase-3/7 Fluorescent staining. Apoptosis of LNCaP95 was increased following NUP210 knockdown (*See* also Fig. S7A). Scale bar = 50 μm. **(E)** Cell cycle analysis. Decrease in S phase and increase in G1 phase following NUP210 knockdown were significant (*See* also Fig. S7B), but not markedly detected compared with SLC3A2 knockdown (Fig. 6). $^{*}P<0.05$ (*t*-test). **(F)** SA-β-Gal staining. The increase of the number of SA-β-Gal(+) cells by NUP210 knockdown was not significantly observed (*See* also Fig. S7C). Scale bar = 50 μm. Data represent the mean ± SEM of 3 experiments.

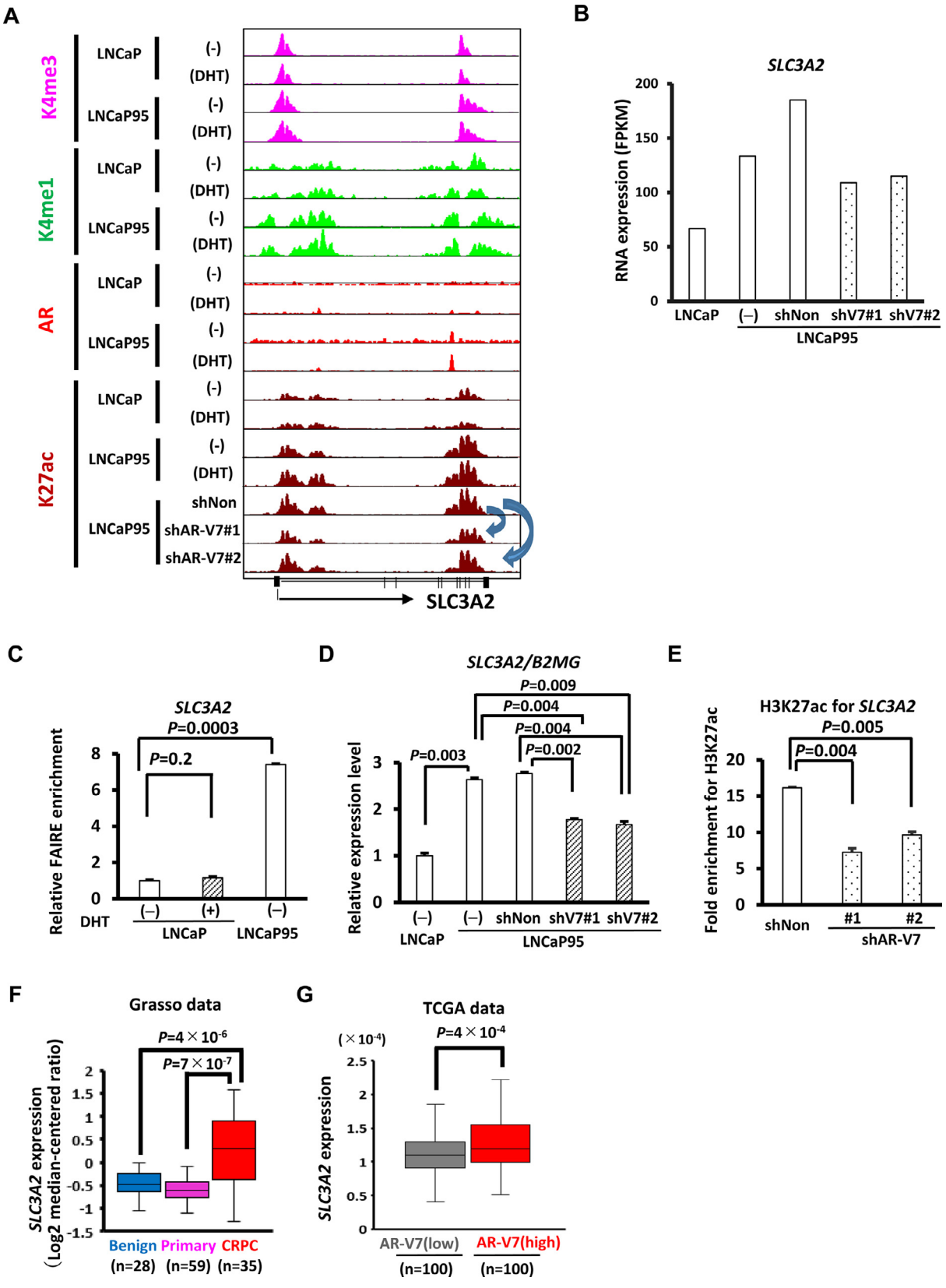

Fig. 5. ***SLC3A2*** **expression in clinical datasets. . (A)** Epigenetic status around *SLC3A2*. AR/AR-V7 binding to *SLC3A2* enhancer and elevated level of H3K27ac signal in LNCaP95 in the absence and presence of DHT were shown. **(B)** RNA expression of *SLC3A2*. AR-V7 knockdown decreased FPKM value of *SLC3A2*. **(C)** FAIRE-qPCR analysis at AR/AR-V7 target region around *SLC3A2* in hormone-depleted or -stimulated LNCaP and hormone-depleted LNCaP95. **(D)** RT-qPCR analysis of *SLC3A2* in LNCaP and LNCaP95 cells with/without shRNA treatment. Downregulation of *SLC3A2* by AR-V7 knockdown was confirmed. **(E)** Reduction of H3K27ac level at the *SLC3A2* enhancer. H3K27ac enrichment was measured by ChIP-qPCR at AR/AR-V7 target region around *SLC3A2*, showing a decrease following AR-V7 knockdown. **(F)** *SLC3A2* expression levels in benign lesions, primary PC, and CRPC, using Grasso prostate dataset. **(G)** *SLC3A2* expression levels in PC cases with higher and lower expression of *AR-V7*, using TCGA PRAD dataset.

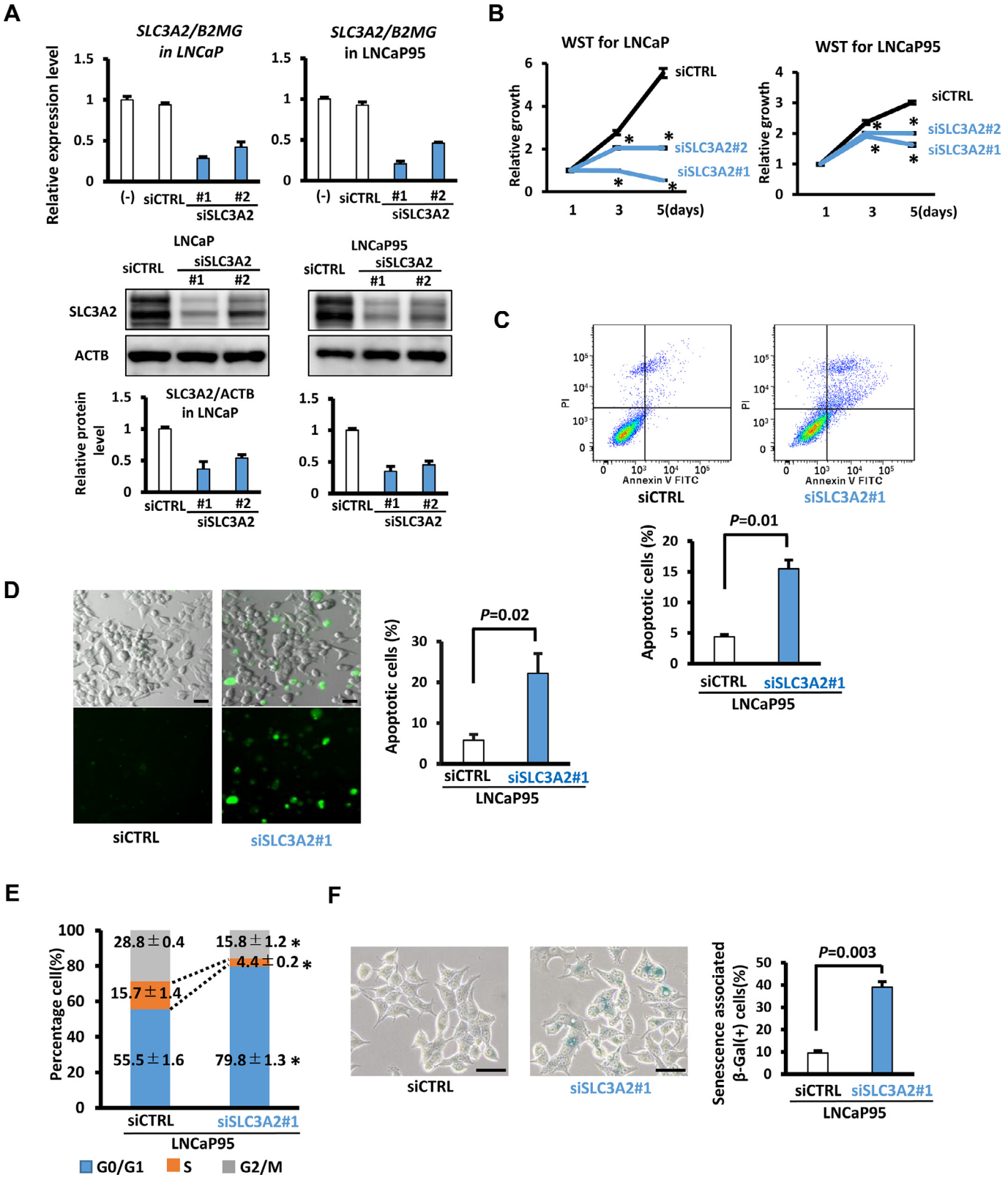

Fig. 6. Growth suppression by SLC3A2 knockdown. LNCaP in presence of androgen and LNCaP95 in absence of androgen were treated with siRNA's against *SLC3A2*. **(A)** (*Upper*) RT-qPCR analysis of *SLC3A2* in LNCaP and LNCaP95 cells following transfection with two siSLC3A2 (*#1* and *#2*). (*Middle*) Western blot analysis of SLC3A2 in LNCaP and LNCaP95 cells following transfection with siSLC3A2. (*Lower*) Quantification of SLC3A2 protein level after normalization to ACTB. **(B)** WST-8 assay for cells following SLC3A2 knockdown. Significant suppression of cellular growth following SLC3A2 knockdown was detected in both LNCaP in hormone-stimulated condition and LNCaP95 in hormone-depleted condition. $^{*}P<0.05$ (*t*-test). **(C)** Cell apoptosis analysis by Annexin-V FITC/PI staining and flow cytometry. The cell apoptosis rate of LNCaP95 was significantly increased following SLC3A2 knockdown. **(D)** Caspase-3/7 Fluorescent staining. Apoptosis of LNCaP95 was increased following SLC3A2 knockdown (*See* also Fig. S7D). Scale bar = 50 μm. **(E)** Cell cycle analysis. Significant decrease in S phase and a significant increase in G1 phase were observed following SLC3A2 knockdown (*See* also Fig. S7E). $^{*}P<0.05$ (*t*-test). **(F)** SA-β-Gal staining. The number of SA-β-Gal(+) cells were increased by SLC3A2 knockdown (*See* also Fig. S7F). Scale bar = 50 μm. Data represent the mean ± SEM of 3 experiments.

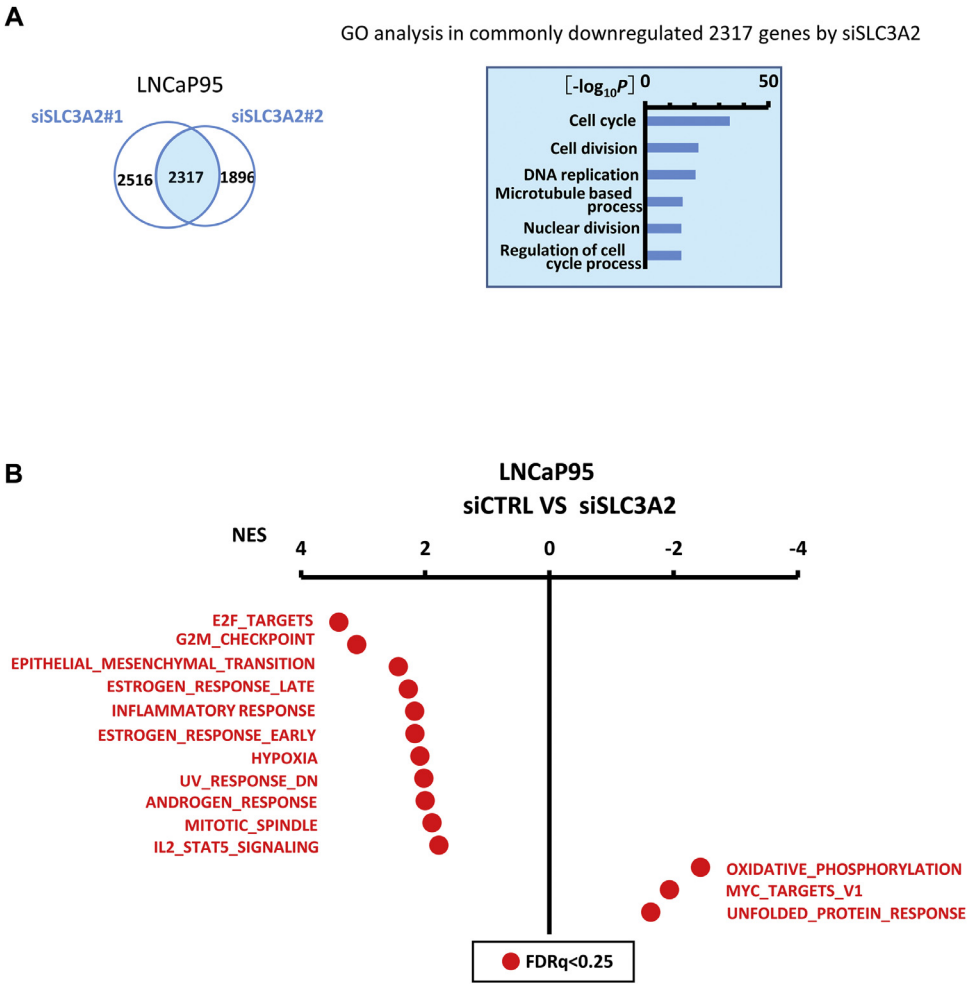

Fig. 7. ***E2F, G2M and EMT pathway inhibition.*** **(A)** Genes downregulated by siSLC3A2#1 and siSLC3A2#2. The 2,317 genes downregulated by siSLC3A2 were significantly associated with GO terms such as cell cycle, cell division and DNA replication. **(B)** Analysis of 50 Hallmark gene sets by GSEA. Genes altered in treatment of LNCaP95 with siSLC3A2 were analyzed. and significantly altered gene sets were shown by *red dots* (FDRq<0.25). Control LNCaP95 cells showed significant upregulation and downregulation in 11 and 3 gene sets, respectively, compared to LNCaP95 treated with siSLC3A2.

expression regulation during chromatin organization [42, 43]. It still remains unknown how NUP210 exerts its function in nuclear pore complexes. While Rajkumar *et al.* reported that NUP210 was upregulated in cervical cancer [44], the role of NUP210 in enhancing tumor aggressiveness is yet to be clarified. Further investigation should be required to determine detailed tumorigenic functions of NUP210.

Limitations of the present study should be noted. First, *in vivo* experiments were not carried out. Second, we have performed these experiments in LNCaP and LNCaP95 cell lines only. Further investigation should be necessary, including *in vivo* experiments and demonstrations by using more cell lines, to confirm the critical roles of the identified AR-V7 target genes.

In summary, we conducted comprehensive ChIP-seq and RNA-seq analyses of LNCaP and LNCaP95 to identify the landscape of AR-V7 target regions, and found that AR-V7 upregulates both AR/AR-V7 common target gene *NUP210* and AR-V7 specific target gene *SLC3A2* that contribute to CRPC proliferation.

Declaration of Competing Interest

The authors declare no competing interests.

Acknowledgment

The authors thank Hisayo Karahi, Eriko Ikeda, and Haruka Maruyama for technical assistance. This work was supported by Japan Agency for Medical Research and Development (AMED) [19ck0106263h0003]; Japan Society for the Promotion of Science [16H05462, 20H03813]; and Chiba University [Global and Prominent Research grant 2018-Y9].

Supplementary materials

Supplementary material associated with this article can be found, in the online version, at doi:10.1016/j.tranon.2020.100915.

References

[1] S.R. L., M.K. D., J. Ahmedin, Cancer statistics, CA: A Cancer J. Clin. 66 (2016) 7–30.
[2] B.J. Feldman, D. Feldman, The development of androgen-independent prostate cancer, Nat. Rev. Cancer 1 (2001) 34–45.
[3] T. Uo, S.R. Plymate, C.C. Sprenger, The potential of AR-V7 as a therapeutic target, Expert Opin. Ther. Targets 22 (2018) 201–216.
[4] P.A. Watson, V.K. Arora, C.L. Sawyers, Emerging mechanisms of resistance to androgen receptor inhibitors in prostate cancer, Nat. Rev. Cancer 15 (2015) 701–711.
[5] S.K. Pal, J. Patel, M. He, B. Foulk, K. Kraft, D.A. Smirnov, P. Twardowski, M. Kortylewski, V. Bhargava, J.O. Jones, Identification of mechanisms of resistance to treatment with abiraterone acetate or enzalutamide in patients with castration-resistant prostate cancer (CRPC), Cancer 124 (2018) 1216–1224.
[6] K. Kita, M. Shiota, M. Tanaka, A. Otsuka, M. Matsumoto, M. Kato, S. Tamada, H. Iwao, K. Miura, T. Nakatani, S. Tomita, Heat shock protein 70 inhibitors suppress androgen receptor expression in LNCaP95 prostate cancer cells, Cancer Sci. 108 (2017) 1820–1827.
[7] D. Robinson, E.M. Van Allen, Y.M. Wu, N. Schultz, R.J. Lonigro, J.M. Mosquera, B. Montgomery, M.E. Taplin, C.C. Pritchard, G. Attard, H. Beltran, W. Abida, R.K. Bradley, J. Vinson, X. Cao, P. Vats, L.P. Kunju, M. Hussain, F.Y. Feng, S.A. Tomlins, K.A. Cooney, D.C. Smith, C. Brennan, J. Siddiqui, R. Mehra, Y. Chen, D.E. Rathkopf, M.J. Morris, S.B. Solomon, J.C. Durack, V.E. Reuter, A. Gopalan, J. Gao, M. Loda, R.T. Lis, M. Bowden, S.P. Balk, G. Gaviola, C. Sougnez, M. Gupta, E.Y. Yu, E.A. Mostaghel, H.H. Cheng, H. Mulcahy, L.D. True, S.R. Plymate, H. Dvinge, R. Ferraldeschi, P. Flohr, S. Miranda, Z. Zafeiriou, N. Tunariu, J. Mateo, R. Perez-Lopez, F. Demichelis, B.D. Robinson, M. Schiffman, D.M. Nanus, S.T. Tagawa, A. Sigaras, K.W. Eng, O. Elemento, A. Sboner, E.I. Heath, H.I. Scher, K.J. Pienta, P. Kantoff, J.S. de Bono, M.A. Rubin, P.S. Nelson, L.A. Garraway, C.L. Sawyers, A.M. Chinnaiyan, Integrative clinical genomics of advanced prostate cancer, Cell 161 (2015) 1215–1228.

[8] B.L. Maughan, E.S. Antonarakis, Clinical relevance of androgen receptor splice variants in castration-resistant prostate cancer, Curr. Treat Options Oncol. 16 (2015) 57.
[9] T. Chandrasekar, J.C. Yang, A.C. Gao, C.P. Evans, Mechanisms of resistance in castration-resistant prostate cancer (CRPC), Transl. Androl. Urol. 4 (2015) 365–380.
[10] Y. Li, S.C. Chan, L.J. Brand, T.H. Hwang, K.A. Silverstein, S.M. Dehm, Androgen receptor splice variants mediate enzalutamide resistance in castration-resistant prostate cancer cell lines, Cancer Res. 73 (2013) 483–489.
[11] E.S. Antonarakis, C. Lu, B. Luber, H. Wang, Y. Chen, Y. Zhu, J.L. Silberstein, M.N. Taylor, B.L. Maughan, S.R. Denmeade, K.J. Pienta, C.J. Paller, M.A. Carducci, M.A. Eisenberger, J. Luo, Clinical significance of androgen receptor splice variant-7 mRNA detection in circulating tumor cells of men with metastatic castration-resistant prostate cancer treated with first- and second-line abiraterone and enzalutamide, J. Clin. Oncol. 35 (2017) 2149–2156.
[12] R. Hu, T.A. Dunn, S. Wei, S. Isharwal, R.W. Veltri, E. Humphreys, M. Han, A.W. Partin, R.L. Vessella, W.B. Isaacs, G.S. Bova, J. Luo, Ligand-independent androgen receptor variants derived from splicing of cryptic exons signify hormone-refractory prostate cancer, Cancer Res. 69 (2009) 16–22.
[13] S.C. Chan, Y. Li, S.M. Dehm, Androgen receptor splice variants activate androgen receptor target genes and support aberrant prostate cancer cell growth independent of canonical androgen receptor nuclear localization signal, J. Biol. Chem. 287 (2012) 19736–19749.
[14] J. Lu, T. Van der Steen, D.J. Tindall, Are androgen receptor variants a substitute for the full-length receptor? Nat. Rev. Urol. 12 (2015) 137–144.
[15] A.A. Igolkina, A. Zinkevich, K.O. Karandasheva, A.A. Popov, M.V. Selifanova, D. Nikolaeva, V. Tkachev, D. Penzar, D.M. Nikitin, A. Buzdin, H3K4me3, H3K9ac, H3K27ac, H3K27me3 and H3K9me3 histone tags suggest distinct regulatory evolution of open and condensed chromatin landmarks, Cells 8 (2019).
[16] R. Hu, C. Lu, E.A. Mostaghel, S. Yegnasubramanian, M. Gurel, C. Tannahill, J. Edwards, W.B. Isaacs, P.S. Nelson, E. Bluemn, S.R. Plymate, J. Luo, Distinct transcriptional programs mediated by the ligand-dependent full-length androgen receptor and its splice variants in castration-resistant prostate cancer, Cancer Res. 72 (2012) 3457–3462.
[17] K. Kita, K. Sugita, C. Sato, S. Sugaya, T. Sato, A. Kaneda, Extracellular release of annexin A2 is enhanced upon oxidative stress response via the p38 MAPK pathway after low-dose x-ray irradiation, Radiat. Res. 186 (2016) 79–91.
[18] A. Kaneda, T. Fujita, M. Anai, S. Yamamoto, G. Nagae, M. Morikawa, S. Tsuji, M. Oshima, K. Miyazono, H. Aburatani, Activation of Bmp2-Smad1 signal and its regulation by coordinated alteration of H3K27 trimethylation in Ras-induced senescence, PLoS Genet. 7 (2011) e1002359.
[19] H. Namba-Fukuyo, S. Funata, K. Matsusaka, M. Fukuyo, B. Rahmutulla, Y. Mano, M. Fukayama, H. Aburatani, A. Kaneda, TET2 functions as a resistance factor against DNA methylation acquisition during Epstein-Barr virus infection, Oncotarget 7 (2016) 81512–81526.
[20] A. Okabe, S. Funata, K. Matsusaka, H. Namba, M. Fukuyo, B. Rahmutulla, M. Oshima, A. Iwama, M. Fukayama, A. Kaneda, Regulation of tumour related genes by dynamic epigenetic alteration at enhancer regions in gastric epithelial cells infected by Epstein-Barr virus, Sci. Rep. 7 (2017) 7924.
[21] K. Matsusaka, S. Funata, M. Fukuyo, Y. Seto, H. Aburatani, M. Fukayama, A. Kaneda, Epstein-Barr virus infection induces genome-wide de novo DNA methylation in non–neoplastic gastric epithelial cells, J. Pathol. 242 (2017) 391–399.
[22] G.P. Dimri, X.H. Lee, G. Basile, M. Acosta, C. Scott, C. Roskelley, E.E. Medrano, M. Linskens, I. Rubelj, O. Pereirasmith, M. Peacocke, J. Campisi, A biomarker that identifies senescent human-cells in culture and in aging skin in-vivo, Proc. Natl. Acad. Sci. USA 92 (1995) 9363–9367.
[23] P.G. Giresi, J. Kim, R.M. McDaniell, V.R. Iyer, J.D. Lieb, FAIRE (Formaldehyde-Assisted Isolation of Regulatory Elements) isolates active regulatory elements from human chromatin, Genome Res. 17 (2007) 877–885.
[24] C.S. Grasso, Y.M. Wu, D.R. Robinson, X. Cao, S.M. Dhanasekaran, A.P. Khan, M.J. Quist, X. Jing, R.J. Lonigro, J.C. Brenner, I.A. Asangani, B. Ateeq, S.Y. Chun, J. Siddiqui, L. Sam, M. Anstett, R. Mehra, J.R. Prensner, N. Palanisamy, G.A. Ryslik, F. Vandin, B.J. Raphael, L.P. Kunju, D.R. Rhodes, K.J. Pienta, A.M. Chinnaiyan, S.A. Tomlins, The mutational landscape of lethal castration-resistant prostate cancer, Nature 487 (2012) 239–243.
[25] J.S. Carroll, X.S. Liu, A.S. Brodsky, W. Li, C.A. Meyer, A.J. Szary, J. Eeckhoute, W. Shao, E.V. Hestermann, T.R. Geistlinger, E.A. Fox, P.A. Silver, M. Brown, Chromosome-wide mapping of estrogen receptor binding reveals long-range regulation requiring the forkhead protein FoxA1, Cell 122 (2005) 33–43.
[26] B. Sahu, M. Laakso, P. Pihlajamaa, K. Ovaska, I. Sinielnikov, S. Hautaniemi, O.A. Janne, FoxA1 specifies unique androgen and glucocorticoid receptor binding events in prostate cancer cells, Cancer Res. 73 (2013) 1570–1580.
[27] C.Y. McLean, D. Bristor, M. Hiller, S.L. Clarke, B.T. Schaar, C.B. Lowe, A.M. Wenger, G. Bejerano, GREAT improves functional interpretation of cis-regulatory regions, Nat. Biotechnol. 28 (2010) 495–501.
[28] Z. Guo, X. Yang, F. Sun, R. Jiang, D.E. Linn, H. Chen, H. Chen, X. Kong, J. Melamed, C.G. Tepper, H.J. Kung, A.M. Brodie, J. Edwards, Y. Qiu, A novel androgen receptor splice variant is up-regulated during prostate cancer progression and promotes androgen depletion-resistant growth, Cancer Res. 69 (2009) 2305–2313.
[29] J. Lu, P.E. Lonergan, L.P. Nacusi, L. Wang, L.J. Schmidt, Z. Sun, T. Van der Steen, S.A. Boorjian, F. Kosari, G. Vasmatzis, G.G. Klee, S.P. Balk, H. Huang, C. Wang, D.J. Tindall, The cistrome and gene signature of androgen receptor splice variants in castration resistant prostate cancer cells, J. Urol 193 (2015) 690–698.
[30] C.C. Feral, N. Nishiya, C.A. Fenczik, H. Stuhlmann, M. Slepak, M.H. Ginsberg, CD98hc (SLC3A2) mediates integrin signaling, Proc. Natl. Acad. Sci. U S A 102 (2005) 355–360.
[31] M. Poettler, M. Unseld, K. Braemswig, A. Haitel, C.C. Zielinski, G.W. Prager, CD98hc (SLC3A2) drives integrin-dependent renal cancer cell behavior, Mol. Cancer 12 (2013) 169.
[32] B. Zhu, D. Cheng, L. Hou, S. Zhou, T. Ying, Q. Yang, SLC3A2 is upregulated in human osteosarcoma and promotes tumor growth through the PI3K/Akt signaling pathway, Oncol. Rep. 37 (2017) 2575–2582.
[33] F. Verrey, E.I. Closs, C.A. Wagner, M. Palacin, H. Endou, Y. Kanai, CATs and HATs: the SLC7 family of amino acid transporters, Pflugers Arch. 447 (2004) 532–542.
[34] R. El Ansari, M.L. Craze, M. Diez-Rodriguez, C.C. Nolan, I.O. Ellis, E.A. Rakha, A.R. Green, The multifunctional solute carrier 3A2 (SLC3A2) confers a poor prognosis in the highly proliferative breast cancer subtypes, Br. J. Cancer 118 (2018) 1115–1122.
[35] O. Yanagida, Y. Kanai, A. Chairoungdua, D.K. Kim, H. Segawa, T. Nii, S.H. Cha, H. Matsuo, J. Fukushima, Y. Fukasawa, Y. Tani, Y. Taketani, H. Uchino, J.Y. Kim, J. Inatomi, I. Okayasu, K. Miyamoto, E. Takeda, T. Goya, H. Endou, Human L-type amino acid transporter 1 (LAT1): characterization of function and expression in tumor cell lines, Biochim Biophys Acta 1514 (2001) 291–302.
[36] M. Xu, S. Sakamoto, J. Matsushima, T. Kimura, T. Ueda, A. Mizokami, Y. Kanai, T. Ichikawa, Up-Regulation of LAT1 during antiandrogen therapy contributes to progression in prostate cancer cells, J. Urol. 195 (2016) 1588–1597.
[37] E. Nakamura, M. Sato, H. Yang, F. Miyagawa, M. Harasaki, K. Tomita, S. Matsuoka, A. Noma, K. Iwai, N. Minato, 4F2 (CD98) heavy chain is associated covalently with an amino acid transporter and controls intracellular trafficking and membrane topology of 4F2 heterodimer, J. Biol. Chem. 274 (1999) 3009–3016.
[38] S. Estrach, S.A. Lee, E. Boulter, S. Pisano, A. Errante, F.S. Tissot, L. Cailleteau, C. Pons, M.H. Ginsberg, C.C. Feral, CD98hc (SLC3A2) loss protects against ras-driven tumorigenesis by modulating integrin-mediated mechanotransduction, Cancer Res. 74 (2014) 6878–6889.
[39] L. Mastroberardino, B. Spindler, R. Pfeiffer, P.J. Skelly, J. Loffing, C.B. Shoemaker, F. Verrey, Amino-acid transport by heterodimers of 4F2hc/CD98 and members of a permease family, Nature 395 (1998) 288–291.
[40] A. Hoelz, E.W. Debler, G. Blobel, The structure of the nuclear pore complex, Annu. Rev. Biochem. 80 (2011) 613–643.
[41] V. Rodriguez-Bravo, R. Pippa, W.M. Song, M. Carceles-Cordon, A. Dominguez-Andres, N. Fujiwara, J. Woo, A.P. Koh, A. Ertel, R.K. Lokareddy, A. Cuesta-Dominguez, R.S. Kim, I. Rodriguez-Fernandez, P. Li, R. Gordon, H. Hirschfield, J.M. Prats, E.P. Reddy, A. Fatatis, D.P. Petrylak, L. Gomella, W.K. Kelly, S.W. Lowe, K.E. Knudsen, M.D. Galsky, G. Cingolani, A. Lujambio, Y. Hoshida, J. Domingo-Domenech, Nuclear pores promote lethal prostate cancer by increasing POM121-Driven E2F1, MYC, and AR nuclear import, Cell 174 (2018) 1200–1215 e1220.
[42] A. Ibarra, M.W. Hetzer, Nuclear pore proteins and the control of genome functions, Genes Dev. 29 (2015) 337–349.
[43] J. Borlido, S. Sakuma, M. Raices, F. Carrette, R. Tinoco, L.M. Bradley, M.A. D'Angelo, Nuclear pore complex-mediated modulation of TCR signaling is required for naive CD4(+) T cell homeostasis, Nat. Immunol. 19 (2018) 594–605.
[44] T. Rajkumar, K. Sabitha, N. Vijayalakshmi, S. Shirley, M.V. Bose, G. Gopal, G. Selvaluxmy, Identification and validation of genes involved in cervical tumourigenesis, BMC Cancer 11 (2011) 80.